Computers and Mathematics with Applications 59 (2010) 2393–2402

Contents lists available at ScienceDirect

Computers and Mathematics with Applications

journal homepage: www.elsevier.com/locate/camwa

A numerical study of temporal shallow mixing layers using BGK-based schemes

Hongwei Liu, Man Yue Lam, Mohamed S. Ghidaoui *

Department of Civil and Environmental Engineering, The Hong Kong University of Science and Technology, Clear Water Bay, Kowloon, Hong Kong

ARTICLE INFO

Keywords:
Mixing layer
Shallow water equations
BGK-based schemes
Large eddy simulation

ABSTRACT

A numerical study of the temporal shallow mixing layers is performed. The depth-averaged shallow water equations are solved by the finite volume method based on the Bhatnagar–Gross–Krook (BGK) equation. The filtering operation is applied to the governing equations and the well-known Smagorinsky model for the subgrid-scale (SGS) stress is employed in order to present a large eddy simulation (LES). The roll-up and pairing processes are clearly shown and the corresponding kinetic energy spectra are calculated. The effects of the Froude number and the bottom friction are numerically investigated. It is shown that the growth rate of the mixing layer decreases as the Froude number increases, which is very similar to the compressible mixing layers when considering the effects of the Mach number. The numerical results also indicate that the increase in bottom friction can enhance the stability of the flows, which is physically reasonable and consistent with the theoretical and experimental findings.

© 2009 Elsevier Ltd. All rights reserved.

1. Introduction

Mixing layer flows can be encountered in aerodynamic, atmospheric, oceanic and hydraulic engineering, where the transverse gradient in the stream-wise velocity makes the flows unstable. The study and understanding of such flows are both theoretically and practically important. According to the Fjortofts theorem [1], instability of the flow is reached in the case of an inflection point in the transverse profile of the stream-wise velocity. Kelvin–Helmholtz instabilities can therefore develop leading to horizontal vortical structures. The wavenumber of the most unstable mode and the growth rate could be predicted to some extent by linear stability analysis; see for example [2,3]. During the past decades, many experimental investigations (for example [4–7]) and numerical studies (such as [8–10]) of mixing layer flows have been carried out, which give more insights into the flows.

Open-channel flows are the turbulent wall flows with a free surface extending over the full water depth; see for example [11] for a review of such flows. A shallow mixing layer can be characterized as a combination of a plane mixing layer flow and an open-channel flow. The flow domain is bounded by a bottom and a free surface and the width of the mixing region is large compared with the water depth. Physically, the bottom of shallow flows gives two-fold effects, one is the drag force which tends to damp the flows, and the other is the small-scale turbulence generated near the bottom. Both of them will affect the horizontal coherent structures. In [12], the spatial shallow mixing layer flow was studied in detail by experiments, analytical modeling and numerical simulation.

A two-dimensional temporal mixing layer was numerically studied and analyzed in [13]. In this paper, the temporal shallow mixing layer flow is investigated by solving the depth-averaged shallow water equations. The filtering operation is applied to the governing equations and the well-known Smagorinsky model [14] for the subgrid-scale stress is employed

* Corresponding author.
E-mail addresses: hwliu@ust.hk (H. Liu), ghidaoui@ust.hk (M.S. Ghidaoui).

0898-1221/$ – see front matter © 2009 Elsevier Ltd. All rights reserved.
doi:10.1016/j.camwa.2009.08.046

in order to present a LES. The numerical method used is the BGK-based finite volume method [15,16], which is an explicit scheme with the second-order accuracy in both time and space.

The rest of the paper is organized as follows. In Section 2, the numerical methodology and the set-up of the problem are described. The numerical results are discussed in Section 3, and the concluding remarks are given in Section 4.

2. Numerical methodology and problem set-up

The filtered shallow water equations can be written as [17,18]

$$\frac{\partial \bar{h}}{\partial t} + \frac{\partial (\bar{h}\hat{\bar{u}}_i)}{\partial x_i} = 0, \tag{1}$$

$$\frac{\partial (\bar{h}\hat{\bar{u}}_i)}{\partial t} + \frac{\partial (\bar{h}\hat{\bar{u}}_i\hat{\bar{u}}_j + \delta_{ij} g\bar{h}^2/2)}{\partial x_j} = -g\bar{h}S_i^b + \frac{\partial}{\partial x_j}[\bar{h}(\nu 2\hat{\bar{S}}_{ij} - T_{ij})] - \frac{\bar{\tau}_i^b}{\rho}, \tag{2}$$

where the hat denotes the depth-averaging operator and the bar represents the filtering operator, $i = 1, 2$ and $j = 1, 2$ with 1 indicating the streaming direction and 2 indicating the cross-stream direction. h is the water depth and u_i is the velocity in x_i direction. g is the gravitational acceleration, S_i^b is the slope of the flow bed along x_i direction. ν is the kinematic viscosity of the fluid, $\delta_{ij} = 1$ when $i = j$ and 0 otherwise. The resolved strain rate tensor $\hat{\bar{S}}_{ij}$ is defined as $\hat{\bar{S}}_{ij} = (\partial\hat{\bar{u}}_i/\partial x_j + \partial\hat{\bar{u}}_j/\partial x_i)/2$. In Eq. (2), ρ is the fluid density, and $\bar{\tau}_i^b$ is the shear stress at the bed of the flow along x_i direction, which can be modeled by the quadratic friction law [14]

$$\bar{\tau}_i^b = \rho c_f \hat{\bar{u}}_i \sqrt{\hat{\bar{u}}_j \hat{\bar{u}}_j}, \tag{3}$$

where c_f is the bed friction coefficient. The subgrid-scale tensor T_{ij} represents stresses acting on the vertical plane over the entire depth due to the combined effects of filtering and depth integration, which can be expressed as

$$T_{ij} = \widehat{\overline{u_i u_j}} - \hat{\bar{u}}_i \hat{\bar{u}}_j. \tag{4}$$

A turbulence model is needed for T_{ij} to close the governing equations. Among various SGS models [19], the simplest and most widely used eddy-viscosity model is proposed by Smagorinsky in [20], where the eddy viscosity ν_t is defined by

$$\nu_t = (C_s \Delta)^2 \left(2\hat{\bar{S}}_{ij}\hat{\bar{S}}_{ij}\right)^{1/2}. \tag{5}$$

This model is employed in our numerical simulation, the Smagorinsky constant C_s is taken as $C_s = 0.065$ [21] and the filter width $\Delta = \sqrt{\Delta x_1 \Delta x_2}$ is adopted.

The filtered shallow water equations are solved by a finite volume method based on the extended BGK equation [15,22]. In this method, the fluxes for the mass and momentum across the surface of the control volume are evaluated from the solution of the BGK equation. The scheme is explicit and second-order in both time and space. It is well known that the Navier–Stokes equations can be obtained from the BGK equation in conjunction with the Chapman–Enskog expansion for low Knudsen number. The direct connection between the unfiltered shallow water equations and the extended BGK model has been established in [15], where the viscous terms in the shallow water equations are recovered from the collision term in the BGK model by setting $\nu = \sigma gh/2$ with σ the collision time. For the filtered shallow water equations, if the eddy-viscosity turbulence model is used for the SGS stress, then the filtered Eqs. (1) and (2) are mathematically equivalent to the classical unfiltered shallow water equations by replacing h, u_i and ν by $\bar{h}$, $\hat{\bar{u}}_i$ and $\nu + \nu_t$, respectively. Thus the BGK-based finite volume method can apply to solve the filtered shallow water equations directly [17]. Detailed derivation and an in-depth analysis of the BGK model for shallow water flows can be found in [15,23].

It should be noted that the BGK-based schemes have been developed and applied to a wide range of flow problems besides the free surface flows, such as the compressible flows [24], near incompressible flows [25], rarefied gas [26] and microscale gas [27] flows. One of the distinguished features for the BGK-based method is that it does not require the operator splitting of the advection and diffusion (both molecular and turbulent) terms, which may be problematic in some circumstances, see for example [28,29]. An interested reader may refer to [30] for a general review of the BGK-based schemes.

The set-up of the problem is given as follows. The gravitational acceleration is taken as $g = 9.8\ \mathrm{ms}^{-2}$ and the slopes of the flow bed are assumed to be zero, i.e. $S_1^b = S_2^b = 0$. The initial mean velocity is given by

$$u_1 = U \tanh\left(\frac{2x_2}{\delta_i}\right) \mathrm{ms}^{-1}, \qquad u_2 = 0, \tag{6}$$

which yields $u_1 = U\ \mathrm{ms}^{-1}$ for $x_2 = +\infty$ and $u_1 = -U\ \mathrm{ms}^{-1}$ for $x_2 = -\infty$. The vorticity thickness δ at any time is defined by

$$\delta(t) = 2U \Big/ \left[\frac{\partial \tilde{u}_1(t, x_2)}{\partial x_2}\right]_{\max}, \tag{7}$$

where $\tilde{u}_1$ denotes the averaged value of u_1 in x_1 direction. The initial vorticity thickness δ_i and the velocity U are taken as $\delta_i = 1$ and $U = 0.2$. The initial water depth h_0 is assumed to be a constant value, which is related to the Froude number Fr by $h_0 = U^2/(gFr^2)$. The kinematic viscosity ν is determined from the Reynolds number Re which is defined by $Re = U\delta_i/\nu$. In our computation, we use $Re = 10^4$.

The initial perturbation superimposed upon the basic velocity field is similar to that in [13]. First, a white-noise stream-function perturbation of small amplitude multiplied by the Gaussian x_2-filter $\exp(-x_2^2/\delta_i^2)$ is superimposed. Second, a further deterministic sine perturbation of wavelength λ_a modulated by the same filter is also superposed on the stream function of the mean flow, where λ_a is the most amplified wavelength given by linear stability analysis, which is approximately $\lambda_a = 7\delta_i$ [2,31]. The amplitudes of the two initial stream-function perturbations (random and deterministic) relative to the stream function of the mean flow are 5×10^{-4}.

In this work we consider a temporal shallow mixing layer with periodic boundary conditions in x_1 direction. The computational domain is a square with the side $D = 4\lambda_a$ in order to obtain four Kelvin–Helmholtz vortices in the stream-wise direction. On $x_2 = \pm D/2$, we employ the free-slip wall boundary conditions. For all our computations, we use uniform Cartesian grid with 256^2 elements in the computational domain. It takes about two hours for a typical run on our desktop (Intel Core 2 Duo E6750 2.67 GHz).

3. Numerical results and discussions

3.1. Evolution of vorticity and water depth fields

Fig. 1 gives the evolution of the vorticity and water depth fields from $t = 0$ to $t = 80\delta_i/U$, where the contour lines of each field are shown. The Froude number is taken as $Fr = 0.1$ in this case, which results in the initial water depth $h_0 = 0.408m$. The bed friction coefficient c_f is given the value $c_f = 10^{-3}$ here. The colors in Fig. 1 indicate the algebraic value from the minimum (blue) to the maximum (red) for both vorticity and water depth. The vorticity of the basic velocity field is negative, so the regions of high vorticity magnitude are given by the blue color and the regions of weak vorticity strength are presented with the red color. For the water depth the blue color corresponds to small h (i.e., low pressure) and the red color large h (i.e., high pressure).

The evolution of the coherent structures are clearly exhibited in Fig. 1: such as the roll-up ($t = 20\delta_i/U$), the first ($t = 40\delta_i/U$) and second pairing ($t = 80\delta_i/U$) processes. The roll-up is the first stage of instability in two-dimensional shear layer. During this stage a dominant wavelength (λ_a here) seems to impose itself as the fastest-growing perturbation at least temporally and to inhibit the growth of perturbations of neighboring wavelengths. The second stage is the successive pairing processes, note that these processes are likely due to the existence of initial subharmonic modes (wavelengths λ_a, $2\lambda_a$, $4\lambda_a$, *etc.*) in the white noise, as discussed in [9]. The subharmonic instability has been theoretically analyzed in [32] and numerically investigated in [33] based on the two-dimensional Navier–Stokes equations. But it has not been investigated for shallow water flows. For the current shallow mixing layers governed by the shallow water equations, we also observe such pairings in our numerical results, which demonstrates the very close relation between these two types of flows. Comparison of the vorticity and water depth fields at the same time ($t > 0$) indicates that the water depth near the center of each eddy is always smaller than that in the outer regions.

3.2. Kinetic energy spectra and vorticity thickness

The statistical quantities such as spectra can provide more information about turbulent flows. Since the mixing layer considered here is periodic in the x_1 direction only, the one-dimensional longitudinal spectrum of the stream-wise fluctuated velocity component u_1' would be more significant physically, which is defined as [13]

$$E_1(k) = \frac{1}{2d}\int_{-d}^{d} \left|\breve{u}_1(\omega_k, x_2)\right|^2 \mathrm{d}x_2, \tag{8}$$

where the longitudinal wavenumber ω_k will be restricted to positive values $\omega_k = 2k\pi/D$, $k = 1, 2, 3, \ldots$, and $2d(\leq D)$ corresponds to a x_2-span on which the longitudinal spectrum is averaged, we choose $2d = D$ in our calculation. $\breve{u}_1(\omega_k, x_2)$ is the longitudinal Fourier transform of the stream-wise fluctuated velocity component u_1' at a given x_2:

$$\breve{u}_1(\omega_k, x_2) = \frac{1}{D}\int_0^D u_1'(x_1, x_2)\exp(-\mathrm{i}\omega_k x_1)\mathrm{d}x_1, \tag{9}$$

with $u_1'(x_1, x_2)$ calculated from

$$u_1'(x_1, x_2) = u_1(x_1, x_2) - \frac{1}{D}\int_0^D u_1(x_1, x_2)\mathrm{d}x_1. \tag{10}$$

Fig. 2 shows the one-dimensional longitudinal spatial energy spectrum $E_1(k)$, which corresponds to the evolution with time of the mixing layer shown in Fig. 1. The small peak ($k = 4$) of the energy spectrum at $t = 0$ represents the sine perturbation (fundamental mode) superimposed upon the white noise (flat spectrum). At time $t = 20\delta_i/U$, the eddies have been

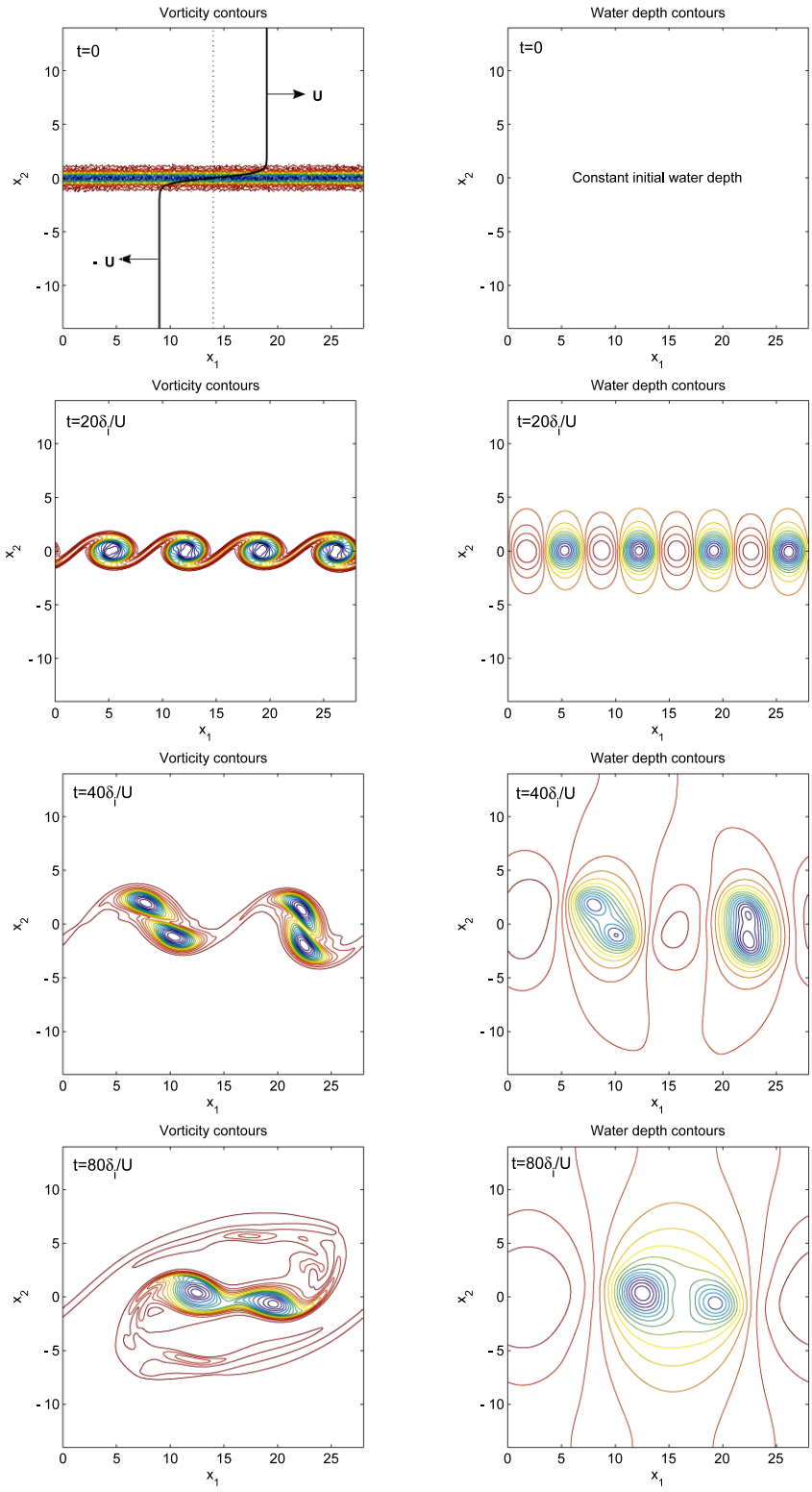

Fig. 1. Contours of vorticity (left) and water depth (right) as time t increases (from top to bottom); the colors indicate the algebraic value from the minimum (blue) to the maximum (red) for both vorticity (negative value) and water depth (positive value). (For interpretation of the references to colour in this figure legend, the reader is referred to the web version of this article.)

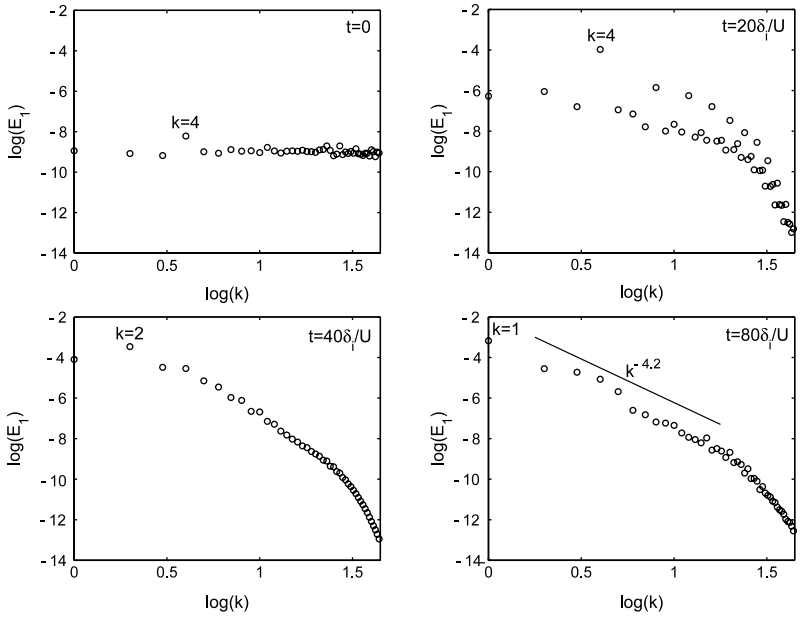

Fig. 2. The one-dimensional longitudinal energy spectra during the evolution of the mixing layer shown in Fig. 1.

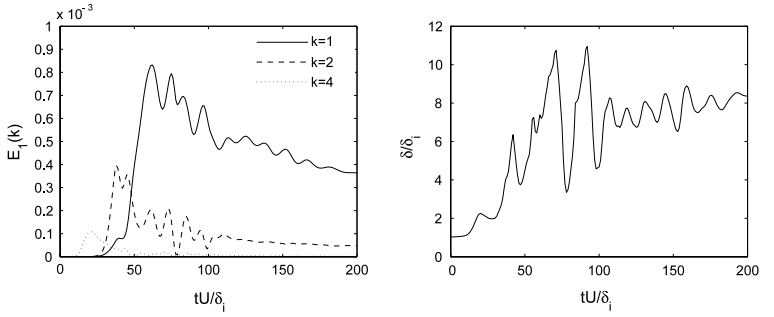

Fig. 3. Evolution of the kinetic energy spectra with time (left) for $k = 1, 2, 4$ and the vorticity thickness (right).

completely formed after the roll-up, which gives a sharp peak of the fundamental mode $k = 4$ and smaller local peaks at its harmonics $k = 8$, 12, 16, and so on. As time increases to $t = 40\delta_i/U$, the first pairing is happening, which makes the mode $k = 2$ grow to a peak in the energy spectrum and the mode $k = 4$ decrease. At time $t = 80\delta_i/U$, as the second pairing, the mode $k = 1$ becomes the largest one in the energy spectrum. The spectral exponent found in our simulations is about -4.2, close to the value of -4 presented in [13], but different from the -3 value found in the classical enstrophy cascade statistical analysis, which is based on the assumption of homogeneous isotropic two-dimensional inviscid flow with no source/sink and thermal effects [34].

Fig. 3 gives the time evolution of the kinetic energy spectra for modes $k = 1$, 2, and 4 and the vorticity thickness δ. From the evolution of these energy spectra, it can be seen that the maximum of $E_1(4)$ happens at about $t = 21\delta_i/U$, when the coherent structures of wavelength λ_a are fully formed. The first pairing occurs at about $t = 38\delta_i/U$, associated with the maximum of $E_1(2)$. The second pairing becomes more complicated due to the confinement effects of the boundaries in x_2 direction, as discussed in [13], which happens at about $t = 70\delta_i/U$ as checked from the vorticity field. From the vorticity thickness evolution in Fig. 3 we can see that the first fundamental eddies have a vorticity thickness of about $2\delta_i$. During the first pairing, the vorticity thickness exhibits a local maximum ($t = 42\delta_i/U$) and a local minimum ($t = 47\delta_i/U$), which correspond to the moments when the alignment of eddies is along cross-stream and stream-wise directions, respectively. The oscillations of vorticity thickness during the second pairing can be explained similarly.

3.3. Effects of the Froude number

In [35] the linear stability analysis of open-channel flows for various Froude numbers has been provided. In order to investigate the effects of the Froude number Fr, we present the results with different Froude numbers $Fr = 0.1, 0.2, 0.3$, and 0.4. For different Froude numbers, we change the initial water depth by the relation $h_0 = U^2/(gFr^2)$, and the bed friction coefficient c_f is changed accordingly so that the initial bed friction parameter S, which is defined as [31]

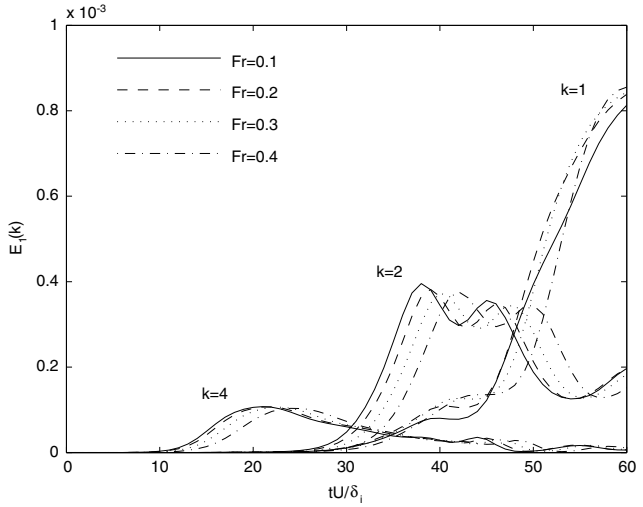

Fig. 4. Evolution of the kinetic energy spectra with time for $k = 1, 2, 4$, with different Froude numbers.

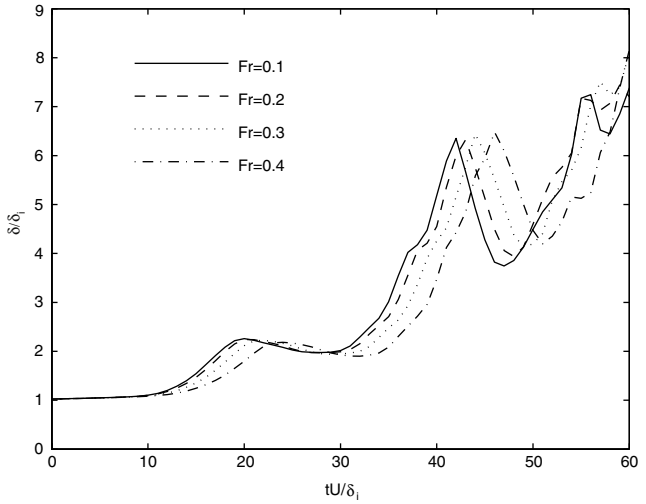

Fig. 5. Evolution of the vorticity thickness with time, with different Froude numbers.

$$S = c_f U / \left(2h_0 \left| \frac{\partial u_1}{\partial x_2} \right|_{\max} \right) = c_f g Fr^2 / \left(U \left| \frac{\partial u_1}{\partial x_2} \right|_{\max} \right), \tag{11}$$

keeps a constant for all these cases. This means the bottom friction effects, which will be discussed in the next section, are equivalent for these cases and the only different condition is the Froude number Fr. The initial velocity field including the two types of perturbations (random and deterministic) is same for all the calculations.

Fig. 4 gives the time evolution of kinetic energy spectra for $k = 1, 2, 4$ and Fig. 5 shows the vorticity thickness evolution. From both figures, we can clearly see that the growth of the shallow mixing layer is delayed as the Froude number Fr increases during the roll-up and first pairing processes (approximately $t \leq 45\delta_i/U$). The boundary confinement effects become more and more important since the end of the first pairing and make the flows more involved. For compressible temporal mixing layers numerical simulations indicate that the growth of the mixing layer is delayed as the convective Mach number M_c increases [36,37], where the convective Mach number M_c is defined by [38]

$$M_c = (U_1 - U_2)/(c_1 + c_2), \tag{12}$$

with U_1 and U_2 being the two free-stream velocities and c_1 and c_2 the sound speeds. Our numerical simulations for the temporal shallow mixing layers also show that the delay of the layer growth is associated with the enhancement of Froude number Fr. Comparison between compressible mixing layer and shallow mixing layer reveals that some strong analogies exist between them. The detailed comparisons and exhaustive discussions between compressible gas flows and hydraulic problems can be found in [39].

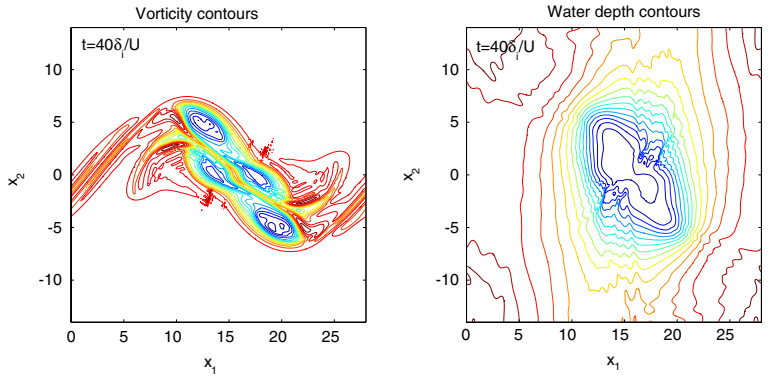

Fig. 6. Contours of vorticity (left) and water depth (right) for the case $Fr = 0.7$.

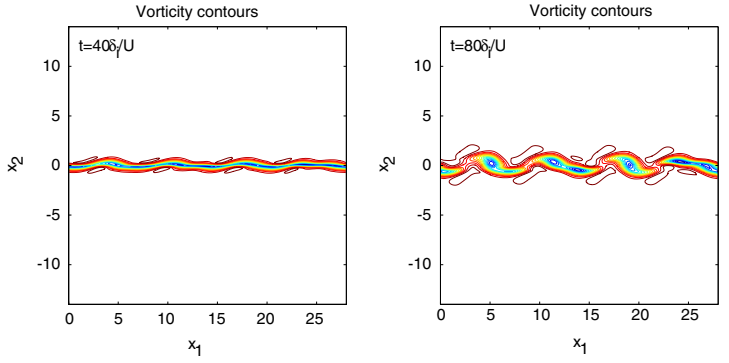

Fig. 7. Contours of vorticity for the case with bed friction parameter $S = 0.0613$.

Spatial mixing layer experiments show that $\delta(x)$ increases linearly with x. For temporal mixing layer the mixing-length theory predicts that $\delta(t) \propto t$ [9], and one can expect to have

$$\frac{\mathrm{d}\delta(t)}{\mathrm{d}t} = \alpha U, \tag{13}$$

where α is a constant, which corresponds to another constant β for spatial mixing layers

$$\frac{\mathrm{d}\delta(x)}{\mathrm{d}x} = \beta \frac{U_1 - U_2}{U_1 + U_2}, \tag{14}$$

where U_1 and U_2 satisfy the relation $U_1 - U_2 = 2U$. We should have $\alpha = \beta$ if the two problems (temporal and spatial) are exactly equivalent. However, from vorticity thickness evolution in Fig. 5 it is found that the mean slope α of the mixing layer growth in our simulations is approximately 0.12, close to that ($\alpha = 0.1$) in [13] but smaller than the value of 0.18 for β observed in various spatial mixing layer experiments [4]. The reason for such difference is still not very clear as discussed in [9].

Both linear stability theory and numerical simulation for compressible time-developing mixing layers [40] indicate that at low Mach number ($M_c < 0.6$) the two-dimensional disturbance is the most unstable mode, while the three-dimensional modes are dominant when $M_c > 0.6$. In our numerical simulations of temporal shallow mixing layer, we also found that the flow develops shock waves embedded around the large-scale vortical structures as the Froude number exceeds some critical value Fr_c, see Fig. 6 for a typical example with $Fr = 0.7$. This phenomena is quite similar to that of compressible mixing layer reported in [41]. Moreover, the critical Froude number Fr_c found in our simulations is approximately $Fr_c = 0.6$. Compared with the compressible flow, again we observe the strong analogies between them.

3.4. Effects of the initial bed friction parameter

For shallow water flows, the bed friction usually tends to suppress the transverse turbulent motion and smooth the flows. In the following, we will study the effects of the initial bed friction parameter S. For the problem considered, we have $S = 0.25c_f/h_0$ from Eq. (11). We consider the case $Fr = 0.1$ ($h_0 = 0.408$ m), then we get the relation $S = 0.613c_f$. By changing the value of c_f, we can vary the initial bed friction parameter S. Figs. 7 and 8 show the vorticity contours for cases

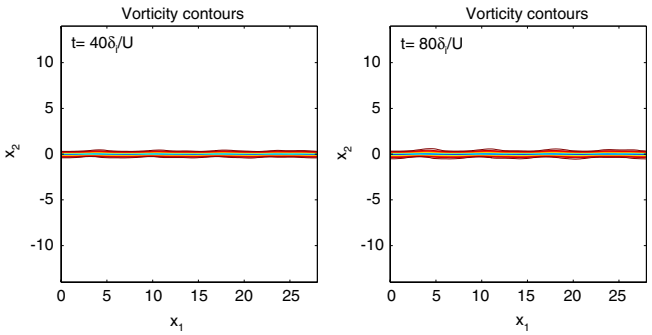

Fig. 8. Contours of vorticity for the case with bed friction parameter $S = 0.1226$.

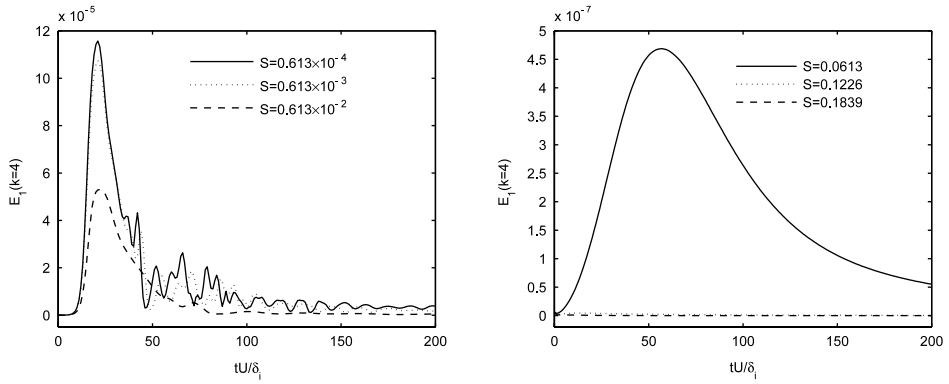

Fig. 9. Evolution with time of the kinetic energy spectra for $k = 4$ with different bed friction parameters.

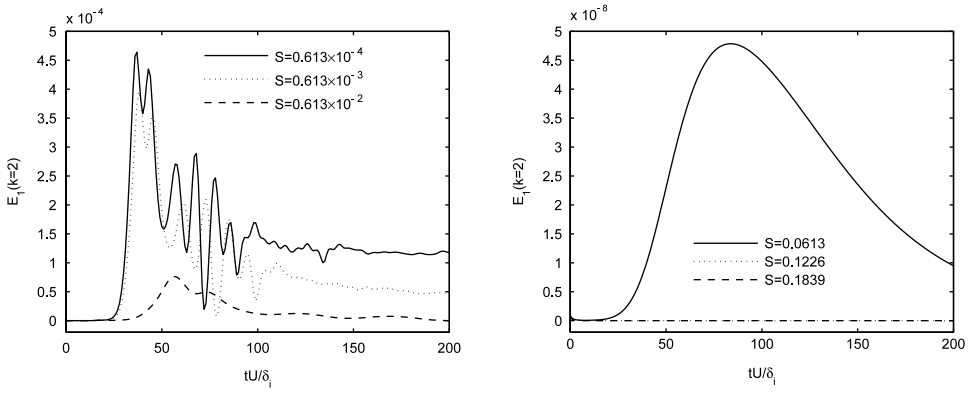

Fig. 10. Evolution of the kinetic energy spectra with time for $k = 2$, with different bed friction parameters.

with $S = 0.0613$ and $S = 0.1226$, respectively. From these figures it can be clearly seen that the flows are more stable with larger bed friction parameter S. Figs. 9–11 give the evolution of kinetic energy spectra with various initial bed friction parameters for $k = 1, 2$, and 4, respectively. These results also indicate that when the initial bed friction parameter exceeds some critical value S_c (around 0.1 in our simulations), the flows are unconditionally stable. This fact was also proved by the theoretical work in [31,35].

4. Conclusions

In this paper, the temporal shallow mixing layers are numerically studied. The BGK-based finite volume method is employed to solve the filtered shallow water equations, and the subgrid-scale dissipation is modeled by the Smagorinsky model. The set-up of the problem is similar to the plane mixing layer investigated in [13]. The numerical results indicate that at the low Froude number, for example $Fr = 0.1$, the shallow mixing layer behaves very similarly to the plane mixing layer shown in [13]. The results of the temporal shallow mixing layers computed with different Froude numbers are also

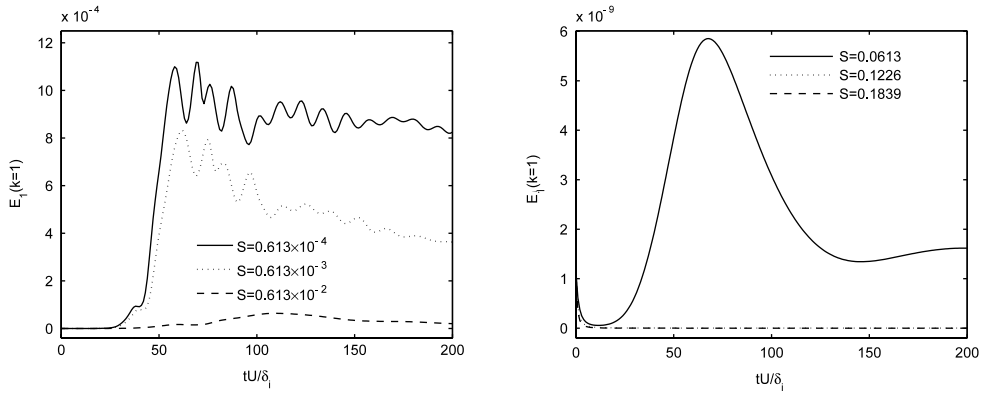

Fig. 11. Evolution of the kinetic energy spectra with time for $k = 1$, with different bed friction parameters.

presented. It is shown by numerical results that the growth rate of the mixing layer decreases as the Froude number increases. Similar phenomena are observed for compressible mixing layer flows when considering the effects of the Mach number. The effects of the bed friction parameter S are also numerically investigated. Our numerical results indicate that the stability of the flows is enhanced as the parameter S increases. When it exceeds some critical value S_c (around 0.1 for our simulations) the flows are unconditionally stable, which is consistent with the theoretical work in [31,35].

Acknowledgements

We are indebted to the anonymous reviewers for their highly constructive comments. The reported work is supported by the Research Grant Council, Hong Kong, under the project No. HKUST6227/04E.

References

[1] P.G. Drazin, W.H. Reid, Hydrodynamic Stability, Cambridge University Press, 1981.
[2] A. Michalke, On the inviscid instability of the hyperbolic tangent velocity profile, J. Fluid Mech. 19 (1964) 543–556.
[3] W. Blumen, Shear-layer instability of an inviscid compressible fluid, J. Fluid Mech. 40 (1970) 769–781.
[4] G.L. Brown, A. Roshko, On density effects and large scale structure in turbulent mixing layers, J. Fluid Mech. 64 (1974) 775–816.
[5] C.D. Winant, F.K. Browand, Vortex pairing: The mechanism of turbulent mixing layer growth at moderate Reynolds number, J. Fluid Mech. 63 (1974) 237–255.
[6] D. Oster, I. Wygnanski, The forced mixing layer between parallel streams, J. Fluid Mech. 123 (1982) 91–130.
[7] M. Zhou, I. Wygnanski, The response of a mixing layer formed between parallel streams to a concomitant excitation at two frequencies, J Fluid Mech. 441 (2001) 139–168.
[8] B. Vreman, B. Geurts, H. Kuerten, Large-eddy simulation of the turbulent mixing layer, J. Fluid Mech. 339 (1997) 357–390.
[9] M. Lesieur, Turbulence in Fluids, Kluwer Academic Publishers, 1997.
[10] E. Balaras, U. Piomelli, J.M. Wallace, Self-similar states in turbulent mixing layers, J. Fluid Mech. 446 (2001) 1–24.
[11] I. Nezu, H. Nakagawa, Turbulence in Open-Channel Flows, in: IAHR Monographs Series, Balkema Rotterdam, 1993.
[12] B.C.van Prooijen, Shallow mixing layers, Ph.D. Thesis, Delft University of Technology, Delft, 2004.
[13] M. Lesieur, C. Staquet, P. Le Roy, P. Comte, The mixing layer and its coherence examined from the point of view of two-dimensional turbulence, J. Fluid Mech. 192 (1988) 511–534.
[14] S.B. Pope, Turbulent Flows, Cambridge University Press, 2000.
[15] M.S. Ghidaoui, J.Q. Deng, K. Xu, W.G. Gray, A Boltzmann based model for open channel flows, Internat. J. Numer. Methods Fluids 35 (2001) 449–494.
[16] K. Xu, A well-balanced gas-kinetic scheme for the shallow water equations with source terms, J. Comput. Phys. 178 (2002) 533–562.
[17] M.S. Ghidaoui, A.A. Kolyshkin, J.H. Liang, F.C. Chan, Q.B. Li, K. Xu, Linear and nonlinear analysis of shallow wakes, J. Fluid Mech. 548 (2006a) 309–340.
[18] C. Hinterberger, J. Frohlich, W. Rodi, Three-dimensional and depth-averaged large-eddy simulations of some shallow water flows, J. Hydr. Engrg., ASCE 133 (8) (2007) 857–872.
[19] M. Lesieur, O. Mtais, Comte P, Large-Eddy Simulations of Turbulence, Cambridge University Press, Cambridge, 2005.
[20] J. Smagorinsky, General circulation experiments with the primitive equations: I. The basic experiment, Mon. Weather Rev. 91 (3) (1963) 99–164.
[21] P. Moin, J. Kim, Numerical investigation of turbulent channel flow, J. Fluid Mech. 118 (1982) 341–377.
[22] M.S. Ghidaoui, J.H. Liang, F.C. Chan, S.Q. Zhang, BGK based finite volume scheme for hydraulic applications, International Journal of Computational Fluid Dynamics 20 (6) (2006b) 439–451.
[23] J.H. Liang, M.S. Ghidaoui, J.Q. Deng, W.G. Gray, A Boltzmann-based finite volume algorithm for surface water flows on cells of arbitrary shapes, J. Hydraul. Res., 45 (2) (2007) 147–164.
[24] H. Liu, K. Xu, A Runge–Kutta discontinuous Galerkin method for viscous flow equations, J. Comput. Phys. 224 (2007) 1223–1242.
[25] Z.L. Guo, H. Liu, L.S. Luo, K. Xu, A comparative study of the LBM and GKS methods for 2D near incompressible flows, J. Comput. Phys. 227 (2008) 4955–4976.
[26] K. Xu, H. Liu, Multiscale gas-kinetic simulation for continuum and near continuum flows, Phys. Rev. E 75 (2007) 016306.
[27] K. Xu, H. Liu, J.Z. Jiang, Multiple temperature kinetic model for continuum and near continuum flows, Phys. Fluids 19 (2007) 016101.
[28] K.H. Karlsen, K.A. Lie, J.R. Natvig, H.F. Nordhaug, H.K. Dahle, Operator splitting methods for systems of convection-diffusion equations: Nonlinear error mechanisms and correction strategies, J. Comput. Phys. 173 (2001) 636–663.
[29] K. Xu, M.L. Mao, L. Tang, A multidimensional gas-kinetic BGK scheme for hypersonic viscous flow, J. Comput. Phys. 203 (2005) 405–421.
[30] K. Xu, A gas-kinetic BGK scheme for the Navier–Stokes equations and its connection with artificial dissipation and Godunov method, J. Comput. Phys. 171 (2001) 289–335.
[31] V.H. Chu, J.H. Wu, R.E. Khayat, Stability of transverse shear flows in shallow open channels, J. Hydr. Engrg., ASCE 117 (10) (1991) 1370–1388.
[32] R.E. Kelly, On the stability of an inviscid shear layer which is periodic in space and time, J. Fluid Mech. 27 (1967) 657–689.

[33] G.M. Corcos, F.S. Sherman, The mixing layer: Deterministic models of a turbulent flow. Part 1: Introduction and the two-dimensional flow, J. Fluid Mech. 139 (1984) 29–65.
[34] R.H. Kraichnan, Inertial ranges in two-dimensional turbulence, Phys. Fluids 10 (1967) 1417–1423.
[35] M.S. Ghidaoui, A.A. Kolyshkin, Linear stability analysis of lateral motions in compound channels with free surface, Journal of Hydraulic Engineering, ASCE 125 (8) (1999) 871–880.
[36] S.K. Lele, Compressibility effects on turbulence, Ann. Rev. Fluid Mech. 26 (1994) 211–254.
[37] A.W. Vreman, N.D. Sandham, K.H. Luo, Compressible mixing layer growth rate and turbulence characteristics, J. Fluid Mech. 320 (1996) 235–258.
[38] D. Papamoschou, A. Roshko, The compressible turbulent mixing layer: An experimental study, J. Fluid Mech. 197 (1988) 453–477.
[39] A.T. Ippen, D.R.F. Harleman, Studies on the validity of the hydraulic analogy to supersonic flow: Parts I and II, USAF Technical Report No. 5985, Hydrodynamics Laboratory, MIT, 1950.
[40] N.D. Sandham, W.C. Reynolds, Three-dimensional simulations of large eddies in the compressible mixing layer, J. Fluid Mech. 224 (1991) 133–158.
[41] N.D. Sandham, W.C. Reynolds, Compressible mixing layer: Linear theory and direct simulation, AIAA J. 28 (1990) 618–624.